Proceedings of the Korean Nuclear Society Meeting
Cheju, Korea, May 2001

Effects of Buffer Thickness on ATW Blanket Performances

Won Sik Yang

Chosun University
375 Seosuk-dong, Dong-gu, Kwangju, Korea, 501-759

Abstract

This paper presents the preliminary results of target and buffer design studies for a lead-bismuth eutectic (LBE) cooled accelerator transmutation of waste (ATW) system, aimed at maximizing the source importance while simultaneously reducing the irradiation damage to fuel. Using an 840 MWt LBE cooled ATW design, the effects of buffer thickness on the blanket performances have been studied. Varying the buffer thickness for a given blanket configuration, system performances have been estimated by a series of calculations using MCNPX and REBUS-3 codes. The effects of source importance change are studied by investigating the low-energy (< 20 MeV) neutron source distribution and the equilibrium cycle blanket performance parameters such as fuel inventory, discharge burnup, burnup reactivity loss, and peak fast fluence. As the irradiation damage to fuel, the displacements per atom (dpa), hydrogen production, and helium production rates are evaluated at the buffer and blanket interface where the peak fast fluence occurs. The results show that the damage rates and the source importance increase monotonically as the buffer thickness decreases. Based on a compromise between the competing objectives of increasing the source importance and reducing the damage rates, a buffer thickness of around 20 cm appears to be reasonable.

I. Introduction

The accelerator-driven systems (ADSs) have been considered in several countries for treating spent fuel and generating power [1]. In these systems, a high-power particle accelerator produces energetic protons that interact with a heavy metal target to produce neutrons. The source neutrons are generated by direct impingement of the accelerator proton beam onto a target material in a process called spallation. The spallation neutrons are subsequently multiplied in the surrounding subcritical blanket. The spallation target and the subcritical blanket are coupled through a buffer region, which helps the spallation neutrons to diffuse into the blanket and reduces the damage to fuel by high-energy neutrons.

The target and buffer designs should be performed in conjunction with the blanket design. The source-driven multiplication factor of a given blanket design increases as the source importance increases. Thus, by designing target and buffer for a higher source importance [2], the desired multiplication factor at the beginning of cycle (which is determined by a compromise between the competing objectives of minimizing accelerator power and precluding the potential for criticality) can be achieved with a reduced amount of fuel. The

reduced fuel loading would increase the discharge burnup for a fixed fuel residence time. This indicates that the target position and the buffer thickness need to be determined such that the source importance is maximized. At the same time, the peak damage to fuel needs to be reduced to increase the fuel residence time and hence the discharge burnup. Therefore, the target position and buffer thickness need to be optimized based on a compromise between these competing objectives.

The effects of buffer thickness on the blanket performances were studied using the 840 MWt LBE-cooled ATW design [3]. Varying the buffer thickness for a given blanket configuration, system performances were estimated by a series of calculations using MCNPX [4] and REBUS-3 [5] codes. The effects of source importance change were studied by investigating the low-energy (< 20 MeV) neutron source distribution and the equilibrium cycle blanket performance parameters such as fuel inventory, discharge burnup, burnup reactivity loss, and peak fast fluence. As the irradiation damage to fuel, the dpa, hydrogen production, and helium production rates were evaluated at the buffer and blanket interface where the peak fast fluence occurs.

The results of these parametric studies are summarized in this paper. Computational model and methods are first described in Section II. The results of parametric studies are discussed in Section III. Specifically, the low-energy neutron source distribution, the equilibrium cycle blanket performance parameters, and the damage rates are compared. Section IV summarizes conclusions and future works.

II. Computational Model and Methods

The effects of buffer thickness on the blanket performances were studied using the 840 MWt LBE-cooled ATW design described in Reference 3. This design was developed to achieve the main objective of high discharge burnup while meeting key thermal-hydraulic and materials-related design constraints. The blanket was assumed to be fueled with a non-uranium metallic dispersion fuel; pyrochemical techniques were used for recycle of residual transuranic actinides (TRU) in this fuel after irradiation. An R-Z model shown in Fig. 1 was used in this study; the blanket region was divided into 3 enrichment zones, 25 depletion regions. In this reference configuration, the LBE target region is 169.6 cm high and 8.5 cm in radius, and is surrounded by a 28.6 cm thick LBE buffer.

The buffer thickness was varied from the reference value to 11.5 cm, while the blanket volume was kept constant. For a 1 GeV proton beam impinging on the top surface of the LBE target with a uniform radial distribution, system performances were estimated by a series of calculations using MCNPX and REBUS-3 codes. A modified version of MCNPX was used in this study. In this modified version of MCNPX, each neutron is killed if its energy is below a user-specified cutoff energy, and its weight, location, direction, and energy are stored on a log file. A low-energy neutron source distribution for a given transmuter configuration can be obtained by processing this log file.

For each buffer configuration, the spallation neutron source distribution was first determined from an MCNPX calculation by setting the neutron cutoff energy to 20 MeV. The beginning of equilibrium cycle (BOEC) compositions obtained from a homogeneous eigenvalue calculation of REBUS-3 was used in this source calculation. By performing a fixed-source REBUS-3 calculation using this low-energy source distribution [6], blanket

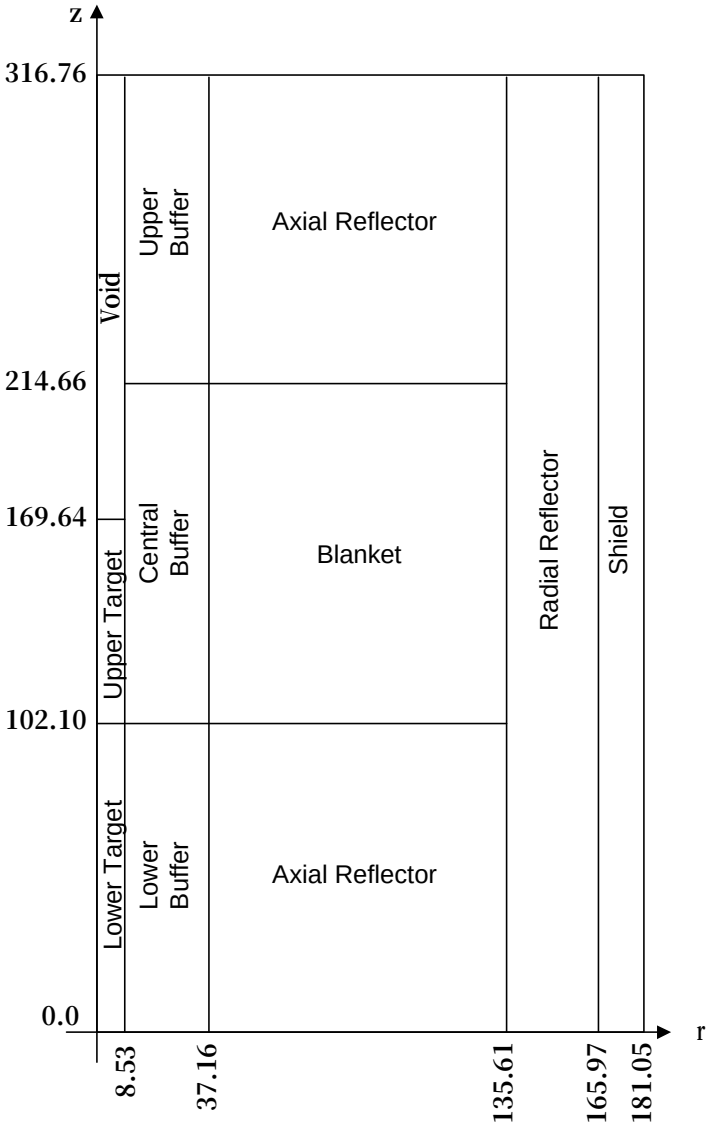

Fig. 1. R-Z Model of 840 MWt LBE Cooled ATW System Design (Base Case)

performances were evaluated for the equilibrium fuel cycle. Assuming a fuel residence time of four years at 75% capacity factor with a cycle length of one half year, the TRU-10Zr particle fraction in fuel was determined such that the source-driven multiplication factor at BOEC is 0.97. In the reference design, the fuel residence time of the innermost fuel assemblies was limited to seven cycles to satisfy the peak fast fluence limit of 4.0×10^{23} n/cm^2. However, this constraint was not imposed in this study, and the fuel residence time was eight cycles for all assemblies. The fuel was depleted at a constant power level by increasing the source intensity over an irradiation cycle to compensate the burnup reactivity loss. The blanket compositions at BOEC and the end of equilibrium cycle (EOEC) were determined from this calculation. Finally, the damage rates of structural material were estimated for the BOEC and EOEC configurations by performing MCNPX calculations with the neutron cutoff energy of zero.

III. Results and Discussions

The effects of buffer thickness on the low-energy (< 20 MeV) neutron source distribution and the equilibrium cycle blanket performance are summarized in Table 1. The low-energy source distributions were generated using 100,000 protons, and the estimated standard deviations for the neutron production per proton were ~0.3%. The source importance factor [2] shown in Table 1 represents the probability for an external neutron to cause a fission reaction relative to a fission neutron. It was estimated by the ratio $(1/k_{eff} - 1)/(1/k_s - 1)$, where k_s is the source-driven multiplication factor determined using the actual flux distribution of the source-driven problem and k_{eff} is the effective multiplication factor obtained from the corresponding eigenvalue calculation.

As shown in Table 1, the number of low-energy source neutrons produced per proton is relatively insensitive to the buffer thickness. The spatial distribution is also insensitive to the buffer thickness. As shown in Fig.2, the radial distributions of low-energy neutron sources at the blanket midplane are practically independent of the buffer thickness. It was also found that the axial distributions at a fixed radius are practically independent of the buffer thickness.

Table 1. Low-Energy Source Distribution and Equilibrium Cycle Blanket Performances

Case	Base	1	2	3	4
Buffer thickness (cm)	28.6	26.8	23.9	18.4	11.5
Relative volume	1.00	0.90	0.75	0.50	0.25
Low-energy neutron source per proton	28.96	28.93	28.85	28.72	28.41
Source neutron distribution (%)					
Upper target	55.30	55.37	55.54	55.83	56.34
Lower target	0.33	0.33	0.32	0.33	0.34
Upper buffer	0.16	0.15	0.14	0.11	0.08
Central buffer	32.90	32.20	30.87	27.78	22.18
Lower buffer	2.62	2.50	2.25	1.73	1.04
Blanket	6.60	7.23	8.43	11.32	16.49
Others	2.09	2.22	2.45	3.40	3.53
Equilibrium cycle performances					
BOEC TRU inventory (kg)	3085	3074	3048	3004	2961
Burnup reactivity loss (%)	5.30	5.24	5.16	5.02	4.87
Discharge burnup (atom %)	28.2	28.3	28.5	28.8	29.2
Peak fast fluence ($\times 10^{23}$ n/cm^2)	4.31	4.44	4.74	5.44	6.64
Power peaking factor					
BOEC	1.358	1.361	1.370	1.386	1.402
EOEC	1.488	1.517	1.584	1.741	2.024
Source importance factor					
BOEC	0.801	0.817	0.843	0.891	0.952
EOEC	0.788	0.803	0.827	0.871	0.926

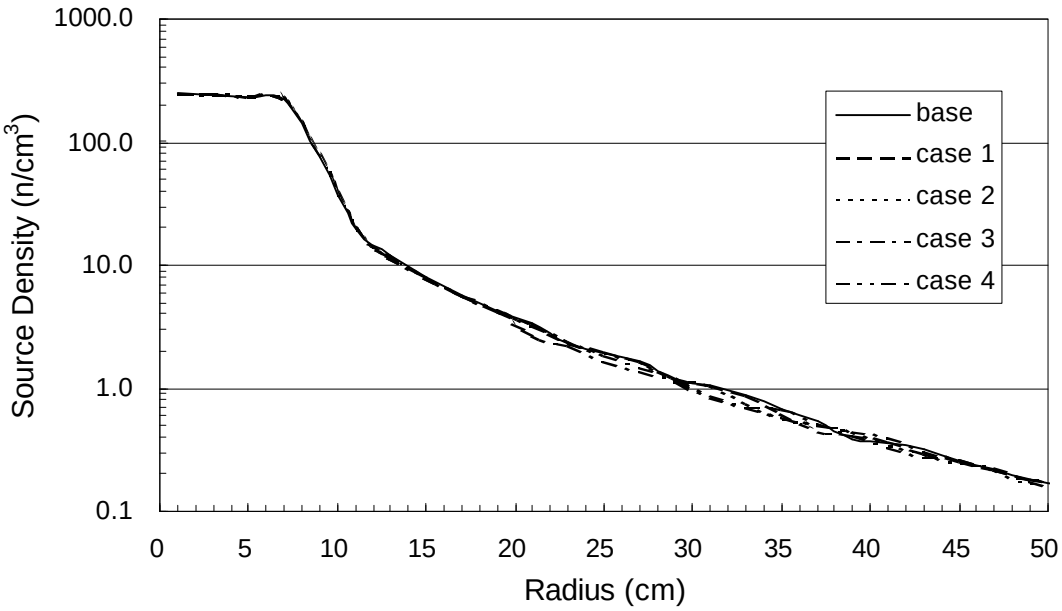

Fig. 2. Radial Distributions of Low-Energy Neutron Sources at Blanket Midplane

These results show that the low-energy neutron source distribution does not depend on the buffer thickness strongly in the range of the buffer thickness considered in this study. However, the number of source neutrons produced in each region strongly depends on the buffer thickness. Among about 29 low-energy source neutrons produced per proton, ~55% are produced in the upper target region that has a relatively small volume, and ~39% are produced in the central buffer and blanket regions. As the buffer thickness decreases, the fraction of source neutrons produced in the central buffer decreases, and that in the blanket increases; however, the sum of two fractions remains almost constant. For example, when the buffer thickness is reduced to 11.5 cm from 28.6 cm, the fraction of low-energy source neutrons produced in the blanket increases by a factor of 2.5. This behavior seems to be due to the leakage of high-energy (> 20 MeV) spallation neutrons into the blanket.

To investigate the effects of secondary neutrons in more detail, separate MCNPX calculations were performed using a cylindrical LBE target with a radius of 20 cm and a height of 100 cm and a practically infinite target. The results showed that a 1 GeV proton directly produced 14.8 neutrons of which about 2.4 neutrons were above 20 MeV. These high-energy neutrons produced 8.8 high-energy neutrons and about 0.7 low-energy neutrons additionally. Among 8.8 high-energy neutrons, about 1.4 neutrons leaked out from the region of 20 cm radius and 100 cm height, and the other neutrons were slowed down below 20 MeV. The neutrons leaking out of the inner region produced 7.8 additional source neutrons in the outer region. These results indicate that high-energy neutrons produce significantly larger number of low-energy source neutrons by successive nuclear interactions. Thus, as the buffer thickness decreases, more high-energy neutrons leak into the blanket and produce additional source neutrons in the blanket region by nuclear interaction or fission. In addition, since the low-energy source neutrons produced in the blanket have higher probabilities to cause a fission reaction than those produced in the other regions, the source importance increases as the buffer thickness decreases.

The results of equilibrium cycle analyses using REBUS-3 show that the BOEC TRU inventory required to achieve a desired source-driven multiplication factor decreases as the

buffer thickness decreases. As a result, the average discharge burnup increases as the buffer thickness decreases. Furthermore, the burnup reactivity loss decreases since the fuel is moved into higher neutron importance region. As shown in Table 1, when the buffer thickness is reduced to 11.5 cm from 28.6 cm, the source importance factor estimated by the diffusion theory increases by ~19%. However, the peak fast fluence and the power peaking factor also increase as the buffer thickness decreases. Especially, the power peaking factor at EOEC increases drastically because of the increased spallation source intensity (to maintain a constant power) and non-uniform TRU depletion. (The peak power density at BOEC occurs in the middle fuel zone due to the enrichment splitting employed to flatten the power distribution, but it moves to the innermost fuel zone at EOEC because of the increased source intensity.)

As discussed in previous studies [7,8], the maximum discharge burnup achievable under various key design constraints is mainly determined by the peak fast fluence limit. Thus, it is desirable to minimize the peak fast fluence per unit discharge burnup. At the same time, the burnup reactivity loss needs to be minimized to reduce the accelerator power or other control requirement. Therefore, for a more consistent comparison, the reactivity loss per unit discharge burnup and the peak fast fluence per unit discharge burnup are compared. As shown in Fig. 3,

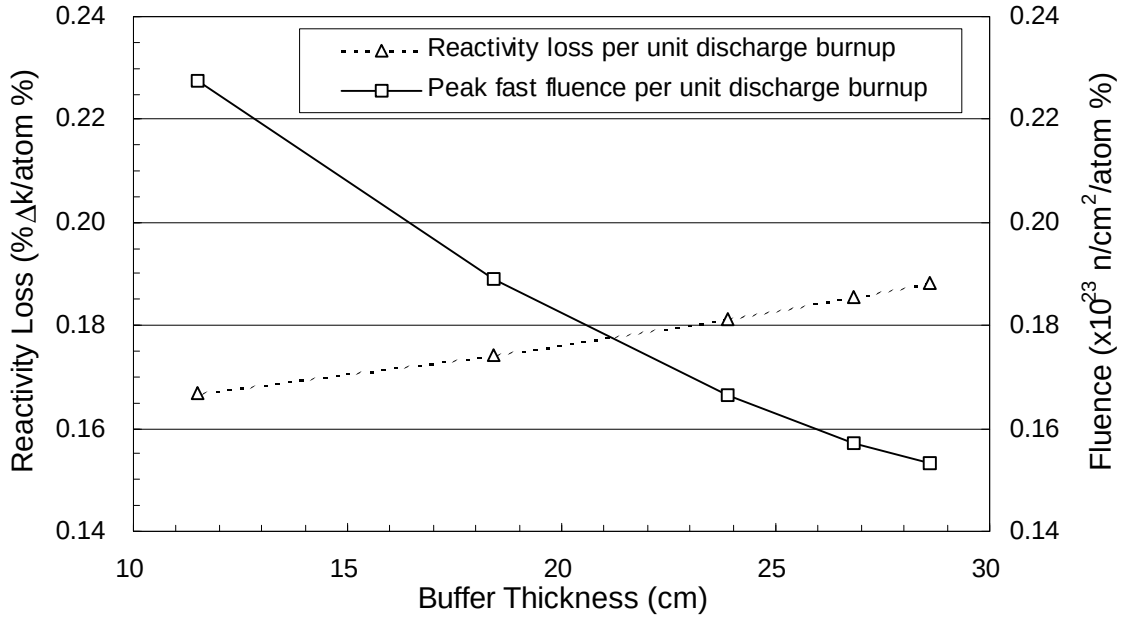

Fig. 3. Burnup Reactivity Loss and Peak Fast Fluence per Unit Discharge Burnup

the reactivity loss per unit discharge burnup decreases monotonically as the buffer thickness decreases. On the other hand, the peak fast fluence per unit discharge burnup increases monotonically. While the burnup reactivity loss per unit discharge burnup decreases almost linearly, the peak fast fluence per unit discharge burnup increases more steeply as the buffer thickness decreases. Based on a compromise between the competing objectives of minimizing the burnup reactivity loss and the peak fast fluence, a buffer thickness of ~20 cm appears to be reasonable.

Table 2 summarizes the effects of buffer thickness on the damage rates of structural material at the buffer and blanket interface. These damage rates (dpa, hydrogen production, and

helium production) at the buffer and blanket interface were determined by renormalizing the results obtained from MCNPX calculations to the power level of 840 MWt. The MCNPX calculations were performed with 1,000 protons in order to limit each computational time to a reasonable amount (~20 hours). The resulting standard deviations of neutron induced damage rates were ~5%, but proton induced ones were typically around 50%. (The standard deviations of proton induced damage rates of the case 1 were close to 100%.) The proton-induced dpa rates

Table 2. Peak Damage Rates of Structural Material at Buffer and Blanket Interface

Case		Base	1	2	3	4
Peak dpa rate of Iron (dpa/year)						
BOEC	Low-energy neutron	42.09	45.90	46.35	51.42	59.50
	High-energy neutron	0.21	0.24	0.29	0.49	1.25
	Sum	42.30	46.14	46.64	51.91	60.75
EOEC	Low-energy neutron	61.36	62.63	68.45	80.77	100.77
	High-energy neutron	0.41	0.41	0.59	1.11	2.37
	Sum	61.77	63.04	69.04	81.88	103.14
Average	Low-energy neutron	51.72	54.27	57.40	66.10	80.14
	High-energy neutron	0.31	0.32	0.44	0.80	1.81
	Sum	52.03	54.59	57.84	66.90	81.94
Peak H production rate (appm/year)						
BOEC	Low-energy neutron (HT9)	35.33	36.29	38.93	53.55	84.86
	High-energy neutron (Fe)	60.58	73.22	112.93	174.17	346.70
	Proton (Fe)	3.88	2.06	5.09	12.32	48.33
	Sum	99.79	111.56	156.94	240.04	479.88
EOEC	Low-energy neutron (HT9)	57.32	61.45	73.68	107.25	204.07
	High-energy neutron (Fe)	128.49	150.48	200.54	377.03	742.90
	Proton (Fe)	4.40	4.10	7.16	31.43	229.40
	Sum	190.21	216.02	281.38	515.71	1176.38
Average	Low-energy neutron (HT9)	46.33	48.87	56.31	80.40	144.47
	High-energy neutron (Fe)	94.54	111.85	156.73	275.60	544.80
	Proton (Fe)	4.14	3.08	6.12	21.87	138.87
	Sum	145.00	163.79	219.16	377.87	828.13
Peak He production rate (appm/year)						
BOEC	Low-energy neutron (HT9)	3.48	3.09	3.82	6.95	11.34
	High-energy neutron (Fe)	3.04	3.66	5.66	8.66	17.55
	Proton (Fe)	0.11	0.07	0.17	0.44	1.75
	Sum	6.63	6.82	9.64	16.05	30.64
EOEC	Low-energy neutron (HT9)	6.93	6.69	8.60	14.16	31.34
	High-energy neutron (Fe)	6.39	7.44	10.09	19.17	38.11
	Proton (Fe)	0.11	0.15	0.27	1.03	8.41
	Sum	13.42	14.28	18.96	34.35	77.86
Average	Low-energy neutron (HT9)	5.20	4.89	6.21	10.55	21.34
	High-energy neutron (Fe)	4.71	5.55	7.87	13.92	27.83
	Proton (Fe)	0.11	0.11	0.22	0.73	5.08

Sum	10.02	10.55	14.30	25.20	54.25

were negligible (less than 0.1%) compared to the neutron induced one, and hence they are not included in Table 2. The low-energy neutron induced hydrogen and helium production rates were evaluated for HT-9, but the others were evaluated for iron.

As shown in Table 2, the dpa of iron is mainly induced by low-energy (< 20MeV) neutrons. However, for the hydrogen and helium production, the high-energy neutron contributions are larger than the others. Especially, the high-energy neutron induced hydrogen production rates are several times larger than the low-energy neutron induced ones. The damage rates increases monotonically as the buffer thickness decreases, since the buffer and blanket interface moves toward a higher flux zone. The damage rates of the case 1 are lower than those of the base case for the hydrogen production rates induced by proton and the helium production rates induced by low-energy neutron and proton, but they are believed to be due to the fluctuation of the source-driven multiplication factor used in the normalization process. In REBUS-3 calculations for determining the fuel particle fraction in the dispersion fuel, the convergence criterion for source-driven multiplication factor was 0.001. As a result, the source-driven multiplication factor at BOEC of the case 1 was larger than that of the base case by 0.1%. However, the source-driven multiplication factor estimated from MCNPX calculations showed a larger fluctuation. The source-driven multiplication factors of the case 1 were larger than those of the base case by 0.3% and 0.4% at BOEC and EOEC, respectively. Thus, the proton beam current required for a constant power was lower for the case 1 than for the base case. Consequently, the damage rates of the case 1 were relatively underestimated.

As shown in Fig. 2, the source density increases exponentially as the distance from the target decreases. Therefore, as the buffer thickness decreases, the innermost fuel zone experiences a much higher flux level and hence a much higher irradiation damage. Furthermore, since the source neutron spectrum is harder than the fission neutron spectrum, the damage rates induced by high-energy neutrons are more severe at reduced buffer thickness. This can be observed from the high-energy damage rates shown in Table 2; the damage rates induced by high-energy neutrons and protons increase much more rapidly as the buffer thickness decreases than those induced by low-energy neutrons. For example, the helium production rates averaged over the cycle show that the damage rates induced by low-energy neutron, high-energy neutron, and proton increase respectively by a factor of 4.1, 5.9, and 45.9 as the buffer thickness is reduced from 28 to 11 cm.

By comparing the peak fast fluence in Table 1 and the dpa rates of iron in Table 2, it can be observed that the dpa is proportional to the fast fluence. These results show that one dpa corresponds to 2.7×10^{21} n/cm^2 (above 0.1 MeV). This is somewhat larger than the value of $\sim 2\times10^{21}$ n/cm^2 observed in EBR-II for 20% cold worked 316 stainless steel cladding [9]. However, these results indicate that the dpa can related to the fast fluence and hence can be estimated using the fast fluence that is easier to calculate.

As discussed above, the peak power density location moves to the innermost fuel zone, and hence the damage rates at the buffer and blanket interface increase over an irradiation cycle. Furthermore, the power peaking factor also increases as the buffer thickness decreases. Especially, the power peaking factor at EOEC increases drastically because of the increased spallation source intensity and non-uniform TRU depletion. As a result, the damage rates at EOEC increase more rapidly as the buffer thickness decreases than the BOEC damage rates. The cycle-averaged total damage rates increase more steeply as the buffer thickness decreases

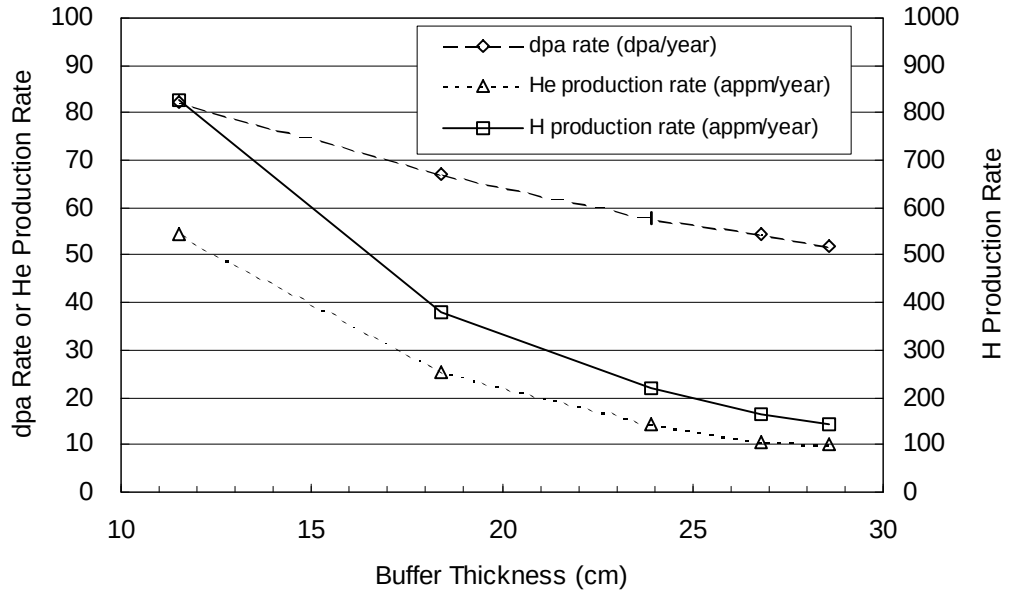

Fig. 4. Cycle-Averaged Damage Rates vs. Buffer Thickness

as shown in Fig. 4. In particular, the hydrogen production rate increases very rapidly when the buffer thickness becomes thinner than ~18 cm.

IV. Conclusions

To summarize the results, the source importance increases significantly (~20%) as the buffer thickness is reduced from 28 to 11 cm; and the burnup reactivity loss also decreases by ~10%. However, the reduced buffer thickness results in large (~50%) increases in the fluence/burnup ratio, implying a much lower discharge burnup for a given fluence limit. In addition, the high-energy damages are much more severe at reduced buffer thickness. Thus, a clear design trade-off between increased accelerator size/cost (thick buffer) and increased fuel processing demand (reduced burnup with thin buffer) is emerging.

Based on the compromise between the competing objectives of increasing the source importance and reducing the irradiation damage, a buffer thickness of ~20 cm appears to be reasonable. However, in order to make more definite conclusions, further studies need to be performed. In particular, it is necessary to investigate the combined effects of various irradiation damage components and to devise the design criteria for the irradiation damage of structural materials using actual irradiation data.

References

1. A Roadmap for developing Accelerator Transmutation of Waste (ATW) Technology; A Report to Congress, DOE/RW-0519, US Dept. of Energy, Oct. 1999.

2. M. Salvatores, I. Slessarev, A. Tchistiakov, and G. Ritter, “The Potential of Accelerator-Driven Systems for Transmutation or Power Production Using Thorium or Uranium Fuel Cycles,” *Nucl. Sci. Eng.*, **126**, 333 (1997).

3. W. S. Yang and H. S. Khalil, "Neutronics Design Studies of an LBE Cooled ATW Blanket," *Proc. of the IAEA Technical Committee Meeting on Core Physics and Engineering Aspects of Emerging Nuclear Energy Systems for Energy Generation and Transmutation*, Argonne, Illinois, USA, Nov. 28 - Dec. 1, 2000.

4. L. S. Walters, "MCNPX Users Manual (Version 2.1.5)," APT Program Report, Los Alamos National Laboratory, November 14, 1999.

5. H. Henryson II, B. J. Toppel, and C. G. Stenberg, "MC^2-2: A Code to Calculate Fast Neutron Spectra and Multigroup Cross Sections," ANL-8144, Argonne National Laboratory (1976).

6. W. S. Yang and H. S. Khalil, "Analysis of the ATW Fuel Cycle Using the REBUS-3 Code System," *Trans. Am. Nucl. Soc*., **81**, 277 (1999).

7. W. Yang and H. Khalil, "Blanket Design Studies of an LBE Cooled Accelerator Transmutation of Waste System, *Nuclear Technology* (to be published).

8. W. S. Yang, D. G. Naberejnev, and H. S. Khalil, "Physics Design Optimization of an LBE Cooled ATW Blanket," *Trans. Am. Nucl. Soc*., **83**, 328 (2000).

9. A. E. Walter and A. B. Reynolds, *Fast Breeder Reactors*, Pergamon Press, Elmsford, New York, U.S.A., (1981).